The GstLAL template bank for spinning compact binary mergers in the second observation run of Advanced LIGO and Virgo

Debnandini Mukherjee,[1, a] Sarah Caudill,[1, 2, b] Ryan Magee,[3, 4] Cody Messick,[3, 4] Stephen Privitera,[5] Surabhi Sachdev,[6] Kent Blackburn,[6] Patrick Brady,[1] Patrick Brockill,[1] Kipp Cannon,[7, 8] Sydney J. Chamberlin,[3, 4] Deep Chatterjee,[1] Jolien D. E. Creighton,[1] Heather Fong,[7] Patrick Godwin,[3, 4] Chad Hanna,[3, 9, 4] Shasvath Kapadia,[1] Ryan N. Lang,[10] Tjonnie G. F. Li,[11] Rico K. L. Lo,[11, 6] Duncan Meacher,[12] Alex Pace,[12] Laleh Sadeghian,[1] Leo Tsukada,[8, 13] Leslie Wade,[14] Madeline Wade,[14] Alan Weinstein,[6] and Liting Xiao[6]

[1]*Leonard E. Parker Center for Gravitation, Cosmology, and Astrophysics,*
University of Wisconsin-Milwaukee, Milwaukee, WI 53201, USA
[2]*Nikhef, Science Park, 1098 XG Amsterdam, Netherlands*
[3]*Department of Physics, The Pennsylvania State University, University Park, PA 16802, USA*
[4]*Institute for Gravitation and the Cosmos, The Pennsylvania State University, University Park, PA 16802, USA*
[5]*Albert-Einstein-Institut, Max-Planck-Institut für Gravitationsphysik, D-14476 Potsdam-Golm, Germany*
[6]*LIGO Laboratory, California Institute of Technology, MS 100-36, Pasadena, California 91125, USA*
[7]*Canadian Institute for Theoretical Astrophysics, 60 St. George Street,*
University of Toronto, Toronto, Ontario, M5S 3H8, Canada
[8]*RESCEU, The University of Tokyo, Tokyo, 113-0033, Japan*
[9]*Department of Astronomy and Astrophysics, The Pennsylvania State University, University Park, PA 16802, USA*
[10]*Hillsdale College, Hillsdale, MI 49242, USA*
[11]*Department of Physics, The Chinese University of Hong Kong, Shatin, New Territories, Hong Kong*
[12]*The Pennsylvania State University, University Park, PA 16802, USA*
[13]*Department of Physics, Graduate School of Science,*
The University of Tokyo, Tokyo, 113-0033, Japan
[14]*Department of Physics, Hayes Hall, Kenyon College, Gambier, Ohio 43022, USA*
(Dated: December 14, 2018)

We describe the methods used to construct the aligned-spin template bank of gravitational waveforms used by the GstLAL-based inspiral pipeline to analyze data from the second observing run of Advanced LIGO and Virgo. The bank expands upon the parameter space covered during the first observing run, including coverage for merging compact binary systems with total mass between $2\,\mathrm{M}_\odot$ and $400\,\mathrm{M}_\odot$ and mass ratios between 1 and 97.989. Thus the systems targeted include merging neutron star-neutron star systems, neutron star-black hole binaries, and black hole-black hole binaries expanding into the intermediate-mass range. Component masses less than $2\,\mathrm{M}_\odot$ have allowed (anti-)aligned spins between ± 0.05 while component masses greater than $2\,\mathrm{M}_\odot$ have allowed (anti-)aligned between ± 0.999. The bank placement technique combines a stochastic method with a new grid-bank method to better isolate noisy templates, resulting in a total of 677,000 templates.

I. INTRODUCTION

The first observing run (O1) of the advanced Laser Interferometer Gravitational-wave Observatory (LIGO) detectors collected data from September 12, 2015 to January 19, 2016, during which two gravitational-wave (GW) signals were detected at greater than 5σ, GW150914 [1] and GW151226 [2] from the mergers of two binary black hole (BBH) systems. The second observing run (O2) of Advanced LIGO ran from November 30, 2016 to August 26, 2017, with Advanced Virgo joining the run for the month of August. To date, GWs from three additional binary black hole mergers [3–5] as well as the low-latency discovery of GWs from a binary neutron star (BNS) merger [6] have been reported from O2.

These types of signals are targeted by all-sky, matched-filter-based searches including GstLAL [7, 8], PyCBC [9–12] and MBTA [13]. Matched-filter-based searches correlate detector data with waveforms predicted by general relativity, drawn from a template bank. The template bank contains waveforms covering a multi-dimensional parameter space of component masses and spins. If a template closely matches a hidden signal in the data, a peak (or trigger) in the correlation time series will be produced. The search pipelines then employ a number of techniques to ensure that triggers are found in operating detectors within the inter-site propagation time and that the signal has the expected morphology and amplitude.

The GstLAL-based inspiral search pipeline (henceforth referred to as GstLAL) operates in two modes, a low-latency online mode and an offline deep-search mode. In this paper, we describe both the template bank used in the online mode for issuing low-latency alerts to astronomy partners as well as the template bank used in the offline mode for the deep analysis of O2 data.

During O1, the matched-filter-based searches of PyCBC and GstLAL used a common template bank with total masses between $2\,\mathrm{M}_\odot$ and $100\,\mathrm{M}_\odot$ [14, 15], to search

for stellar-mass binary black holes. For O2, separate banks were constructed and utilized [16], to enhance the independence of search-pipeline results. Additionally, for O1, a separate search for GWs from intermediate-mass black hole binaries (IMBHB) was performed using a template bank with total mass between $50\,\mathrm{M_\odot}$ and $600\,\mathrm{M_\odot}$ [17]. The IMBH search thus partially overlapped the stellar-mass search in the mass range between $50\,\mathrm{M_\odot}$ and $100\,\mathrm{M_\odot}$, resulting in complexities in assigning significances to candidate events recovered by both searches with differing sensitivities. Hence, for O2, an integrated search was implemented with a template bank covering total masses up to $400\,\mathrm{M_\odot}$.

The paper is organized in the following way. In Section II we describe the design and construction of the integrated template bank used by GstLAL for the analysis of O2 data. In Section III we describe the performance of the bank in recovering simulated signals from a variety of astrophysical populations. We present our conclusions in Section IV.

II. DESIGN AND CONSTRUCTION OF THE O2 BANK

A. Astrophysical source targets

The O2 GstLAL search targeted GW signals from merging binary compact objects with component masses between $1\,\mathrm{M_\odot}$ and $399\,\mathrm{M_\odot}$. These include binary systems with two neutron stars (BNS), two black holes (BBH), or a neutron star and a black hole (NSBH). This component mass region is known to be populated with compact objects produced from the collapse of massive stars. With stellar evolution models, neutron stars can form in the mass range between $1\,\mathrm{M_\odot}$ and $3\,\mathrm{M_\odot}$ [18–22] although there is only one observed neutron star with a mass larger than $2\,\mathrm{M_\odot}$ [23], and those in binaries do not approach $2\,\mathrm{M_\odot}$ [24]. Stellar evolution models also predict that black holes may exist with a minimum mass down to $2\,\mathrm{M_\odot}$ [25] and a maximum mass up to $100\,\mathrm{M_\odot}$ or potentially higher [26, 27]. Black holes with masses between $\sim 100\,\mathrm{M_\odot}$ and $\sim 10^5\,\mathrm{M_\odot}$ are classified as intermediate-mass black holes and could have formed through hierarchical merging of lower mass black holes [28]. This search is also sensitive to GWs from binaries of primordial black holes (PBH), formed from over-dense regions in the early universe. However, distinguishing a PBH GW signal from a conventional stellar-evolution black hole GW signal would not be possible with this search and is instead pursued in a separate search of the sub-solar mass region [29].

We also define different ranges of allowed angular momentum for component neutron stars and component black holes. We consider only the dimensionless spin $\chi = c\left|\vec{S}\right|/Gm^2$ where $\vec{S}$ is the angular momentum and m is the component mass. Observations of the fastest spin-

ning pulsar constrain $\chi \lesssim 0.4$ [30] while pulsars in binaries have $\chi \leq 0.04$ [31]. X-ray observations of accreting BHs indicate a broad distribution of BH spins [32–34], while the relativistic Kerr bound $\chi \leq 1$ gives the theoretical constraint [35].

These observations and evolution models inform the ranges of parameters we define for our template banks. As shown in Fig. 1, we can see the BNS, NSBH, and BBH populations represented in the O2 GstLAL offline search. We impose an additional constraint on the component dimensionless spins of template waveforms by requiring their orientations to be aligned or anti-aligned with the orbital angular momentum of the binary $\hat{L}$. Then the dimensionless projections of the component spins along $\hat{L}$ are defined as $\chi_i \equiv c\left|\vec{S}_i \cdot \hat{L}\right|/Gm_i^2$. The region in green marks the BNS templates with component masses between $1\,\mathrm{M_\odot}$ and $2\,\mathrm{M_\odot}$ and (anti-)aligned dimensionless spin magnitudes with $\chi_{1,2} < 0.05$. This χ limit is motivated by the observational limit of $\chi \leq 0.04$ but with some added uncertainty. The region in blue marks the BBH templates with component masses between $2\,\mathrm{M_\odot}$ and $399\,\mathrm{M_\odot}$ and (anti-)aligned dimensionless spin magnitudes with $\chi_{1,2} < 0.999$. This χ limit is chosen to be as close to the theoretical limit of 1 as possible with current waveform approximants, as described in Section II B 2. The templates in red mark the NSBH range with the neutron star mass between $1\,\mathrm{M_\odot}$ and $2\,\mathrm{M_\odot}$ and the black hole mass between $2\,\mathrm{M_\odot}$ and $200\,\mathrm{M_\odot}$. For these systems, neutron stars have $\chi_{1,2} < 0.05$ and black holes have $\chi_{1,2} < 0.999$.
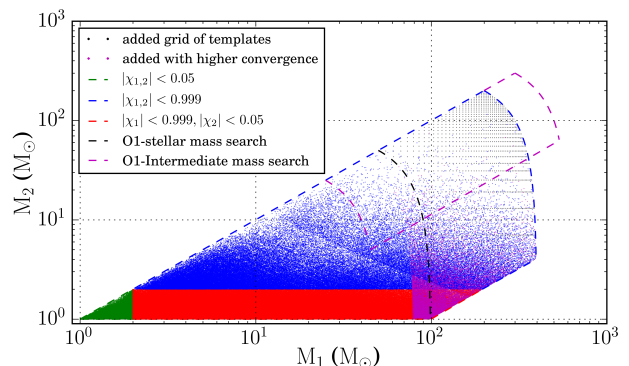

FIG. 1. The template bank used by the O2 GstLAL offline search in component mass space. The templates representing the different astrophysical populations are shown in green for BNS, blue for BBH, and red for NSBH.

In Fig. 2, we can see the BNS, NSBH, and BBH populations represented in the O2 GstLAL online search. The BNS templates cover the same component mass and dimensionless spin magnitude range as the offline bank. However, a cut on total mass results in different mass ranges for NSBH and BBH templates. The maximum allowed total mass is $150\,\mathrm{M_\odot}$, to remove high-mass templates which correspond to short waveforms that recover

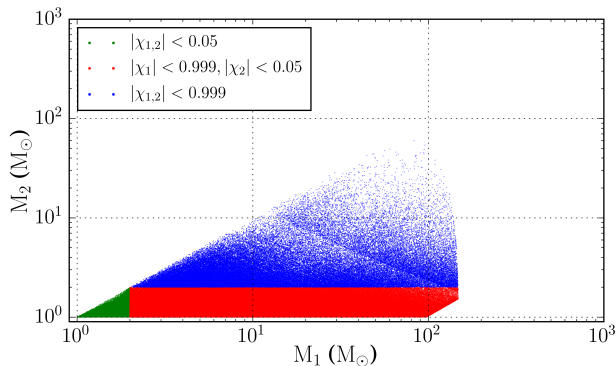short transient noise fluctuations (glitches) at a high rate.

FIG. 2. The template bank used by the O2 GstLAL online search in component mass space. The templates representing the different astrophysical populations are shown in green for BNS, blue for BBH, and red for NSBH.

B. Construction of the O2 bank

The construction of a template bank relies on a number of parameters, including the selection of a representative noise power spectral density $S_n(f)$ and appropriate waveform models, the waveform starting frequency f_{low}, the placement method, and a specified minimum fitting factor criteria [36–38] for all templates in the bank.

The minimum fitting factor describes the effectualness of a template bank in recovering astrophysical sources. To define this quantity, we note that the matched filter output is maximized when a template waveform exactly overlaps the signal waveform. This optimization is impossible in practice, however, since the template bank samples the parameter space discretely while astrophysical sources arise from a continuum. Regardless, it is useful to quantify the degree to which two waveforms, h_1 and h_2, overlap. The overlap is defined as the noise-weighted inner product integral:

$$(h_1|h_2) = 2 \int_{f_{\text{low}}}^{\infty} \frac{\tilde{h}_1(f)\tilde{h}_2(f) + \tilde{h}_1(f)\tilde{h}_2(f)}{S_n(f)} df, \qquad (1)$$

where f_{low} was set to 15 Hz, as motivated by the noise power spectral density described in Section II B 1.

The *match* between two waveforms is then defined as the maximization over coalescence phase and time of the noise-weighted inner product:

$$M(h_1, h_2) = \max_{\phi_c, t_c} (h_1|h_2(\phi_c, t_c)) \qquad (2)$$

This defines the percent of signal-to-noise ratio (SNR) retained when recovering waveform h_2 with the (non-identical) waveform h_1. Then, the fitting factor is the related quantity used in describing the effectualness of template banks:

$$FF(h_s) = \max_{h \in \{h_b\}} M(h_s, h) \qquad (3)$$

where h_b is the set of templates in the bank and h_s is a signal waveform with parameters drawn from the continuum. The fitting factor describes the fraction of SNR retained for arbitrary signals in the parameter space covered by the bank. Typically, compact binary coalescence searches have required a fitting factor of 97% to ensure that no more than $\sim 10\%$ of possible astrophysical signals are lost due to the discrete nature of the bank. As described in Sect. II B 3, we use a hierarchical set of fitting factor requirements to construct the bank.

1. Modeling the detector noise

The noise power spectral density (PSD) as shown in Fig. 3 was used to compute the overlap integrals in the construction of the O2 template bank. This projected O2 sensitivity curve was produced by combining some of the best LIGO L1 sensitivities achieved before the start of O2. At low frequencies, below 100 Hz, the best sensitivity is taken from L1 measurements during commissioning in February 2016. At high frequencies, above 100 Hz, the best sensitivity is taken from L1 during O1, with projected improved shot noise due to slightly higher input power and improved efficiency of the readout chain. Calculation of this PSD has been documented in [39].
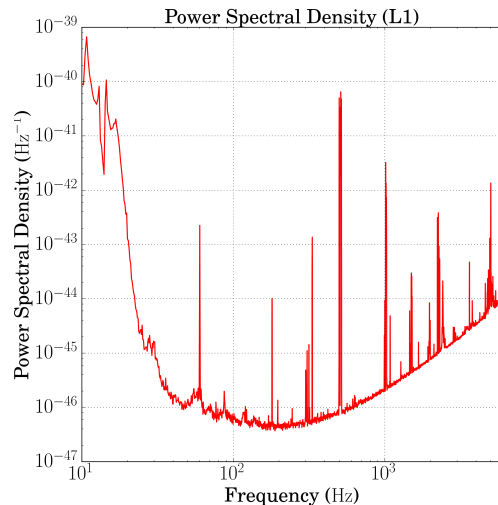

FIG. 3. Representation of the model power spectral density of detector noise. This was used to construct the O2 template bank.

2. *Waveform approximants*

Gravitational waveforms from compact binary mergers are described by 17 intrinsic and extrinsic parameters. However, as demonstrated in [40], for template placement purposes, we can parameterize these systems by three parameters composed of component masses m_i and the reduced-spin parameter χ which is a function of the dimensionless spin parameters χ_i for $i = 1, 2$.

Above a total mass of $4\,\mathrm{M_\odot}$, the waveforms of the binary systems are approximated by an effective-one-body formalism (SEOBNRv4_ROM) [41], combining results from the post-Newtonian approach, black hole perturbation theory and numerical relativity to model the complete inspiral, merger and ringdown waveform. Below a total mass of $4\,\mathrm{M_\odot}$, the binary systems are approximated by an inspiral waveform accurate to third-and-a-half post-Newtonian order called the TaylorF2 waveform model [14, 42]. The extent of the present parameter space covered by the template bank is limited by the availability of waveform models and the sensitivity of the present search. We neglect the effect of precession and higher order modes in our templates.

3. *Template placement*

Both the O2 offline and online template banks were created in the same way, by constructing two sub-banks that were added together. For systems with total mass $2\mathrm{M_\odot} \leq M \leq 4\mathrm{M_\odot}$ where the TaylorF2 approximant is used, the templates were first laid out using a geometric metric technique [43]. This geometric bank was used as a coarse seed bank for an additional stochastic method placement [40, 44] with a convergence threshold set to 97%. For systems with total mass greater than $4\,\mathrm{M_\odot}$, where the SEOBNRv4_ROM approximant is used, a coarse bank was first generated with the stochastic method but with a very low convergence threshold. Again this stochastic bank was used as a coarse seed bank for an additional stochastic method placement with a convergence threshold set to 97%. Additionally, only waveforms with a duration longer than $0.2\,\mathrm{s}$ were retained, to avoid recovering short transient noise glitches. The two sub-banks were added to form the full bank with a total of 661,335 templates.

The original O2 offline bank, as shown in Fig. 4 aided in the discovery of one of the earliest events detected during O2, GW170104 [3]. The higher density of the bank at lower masses is expected because low mass systems have longer waveforms and spend more time in the detectors' sensitive frequency band. This enables the matched-filter search to better distinguish between two different low mass systems. This also means that more templates are required in the lower mass region of the bank for the required fitting factor convergence. At the highest masses, the waveforms contain very few cycles and very few templates are required for coverage in this region.
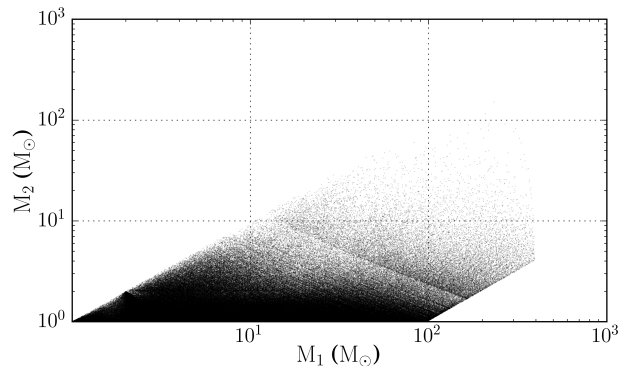

FIG. 4. A visual representation of the original O2 bank in the component mass space, containing a total of 661,335 templates placed with a minimal match of 97%.

Early in O2, short duration glitches were found to be particularly problematic for the online search, even with a duration cut of $0.2\,\mathrm{s}$ applied. Thus, to avoid delays in delivering low-latency gravitational-wave triggers, only waveforms with a total mass $< 150\,\mathrm{M_\odot}$ were retained in the online bank. This online bank, as shown in Fig. 2, was used for the entirety of the O2 observing run.

4. *Overcoverage in the offline bank*

As outlined in Section II C, templates are grouped by the GstLAL search so that each group has the same number of templates with similar parameters and background noise characteristics [7, 45]. It was uncovered partway through O2 that the lower density of templates in the high mass part of the offline bank was resulting in templates with very different background noise properties being grouped together. This led to incorrect averaging of noise properties in the high mass groupings of templates and, in turn, resulted in incorrect estimation of the significance of loud coincident noise in time-shifted data from the two detectors [45]. This was not an issue in the online bank due to the cut at total mass $> 150\,\mathrm{M_\odot}$.

Two different recourses were taken. The offline bank was overpopulated with extra templates in the higher mass region as outlined below. Additionally, the templates in this part of the bank were grouped differently from those in the denser lower mass region such that templates with more similar noise characteristics can be grouped together. Details of the template grouping methods are given in Ref. [45], which is to be published soon.

Regarding the overcoverage, extra templates were added to the initial offline bank in the total mass range of $80\mathrm{M_\odot} \leq M \leq 400\mathrm{M_\odot}$ using two methods. As a first step, the original offline bank was used as a seed for an additional stochastic placement in the total mass range $80\mathrm{M_\odot} \leq M \leq 400\mathrm{M_\odot}$ with an increased convergence threshold of 98%. Additionally, no template duration

threshold was used so as to not exclude the short waveforms corresponding to the heavier mass systems. A total of 14,665 templates, as shown in Fig. 5, were added to the initial offline bank.

Despite the increased convergence threshold, the high mass region of the bank remained sparsely populated, as the overlap between high mass waveforms with few cycles are generally high. Thus, the convergence threshold is already met, without the placement of additional templates. However, short duration glitches are also recovered by a relatively few number of high mass templates, and if these few glitchy templates are grouped together for background estimation with quieter templates, they can spoil the sensitivity over a broad mass range. Thus, we chose to force the placement of additional templates at higher mass using a uniform grid placement in component mass space for the total mass range between $100\text{M}_\odot \leq M \leq 400\text{M}_\odot$, with mass ratios between 1 and 97.989. A total of 1000 templates were placed without any limitations on the waveform duration. This gridded bank, as shown in Fig. 6, was then added to the offline bank produced in the previous step.
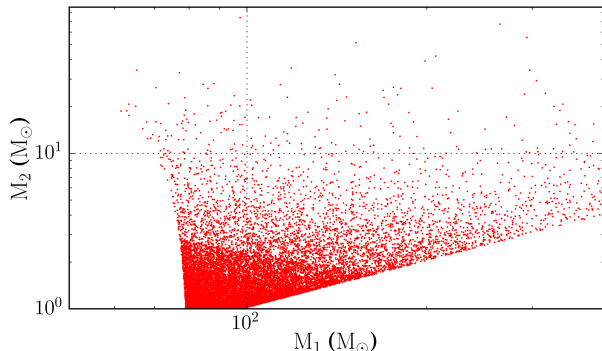

FIG. 5. The bank of extra 14,665 templates that were added to the initial O2 bank, with a 98% minimum match above a total mass of 80 $\text{M}_\odot$ in the component mass space.
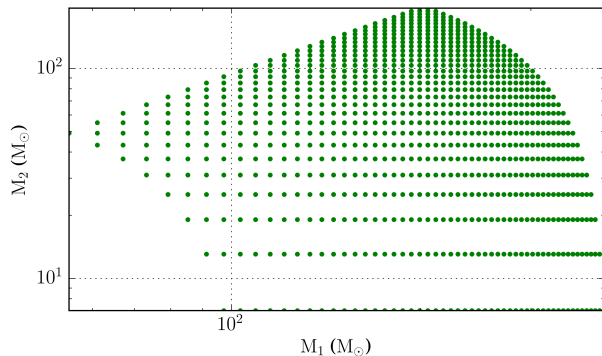

FIG. 6. The uniform grid bank with a 1000 templates spanning 100-400 $\text{M}_\odot$ in total mass .

All together, the final, improved O2 bank has a total of about 677,000 templates, as shown in Fig. 1.

C. Implementation in the GstLAL pipeline

The GstLAL-based inspiral search is a matched-filtering pipeline. The noise-weighted inner product of each whitened template with the whitened data produces the signal-to-noise ratio (SNR). Both signals and glitches can produce high SNR, thus a number of additional consistency and coincidence checks are implemented in the pipeline, as detailed in Ref. [45]. In order to access the full waveform of systems up to $400\,\text{M}_\odot$ that merge at lower frequencies, the filtering frequency was reduced from 30 Hz in the O1 search to 15 Hz.

For the purpose of background estimation, templates are grouped together so that each group has the same number of templates with similar background noise characteristics. Noise properties are averaged separately for each group. Prior to O2, templates were grouped according to two composite parameters that characterize the waveform inspiral to leading order. These were the chirp mass of the binary $\mathcal{M}$ and the effective spin parameter χ_{eff}. The chirp mass is

$$\mathcal{M} = \frac{(m_1 m_2)^{3/5}}{(m_1 + m_2)^{1/5}}. \tag{4}$$

The effective spin parameter is defined as

$$\chi_{\text{eff}} \equiv \frac{m_1 \chi_1 + m_2 \chi_2}{m_1 + m_2}, \tag{5}$$

and acts as a mass-weighted combination of the spin components (anti-)aligned with the total angular momentum.

However, as described in Sect. II B 4, extra templates were placed in the high mass region of the offline bank, to better capture the properties of the noise in that regime. Templates above a total mass of $80\,\text{M}_\odot$ were then grouped by template duration from 15 Hz rather than the $\mathcal{M}$ and χ_{eff} binning used at lower masses. Template duration better characterizes the waveform merger and ringdown, the detectable part of the signal for high mass systems.

III. EFFECTUALNESS

To assess the effectualness of this template bank, we compute again the FF(h_s) as defined in Eq. 3 for a collection of simulated signals with parameters drawn randomly from the covered mass and spin space. The FF depends on a number of parameters including masses, spins, spin orientations and sky locations. Hence it is often represented and plotted as a function of two such parameters. In order to do so, the FF is binned in the two parameters and the average or mean FF in each bin is plotted [37]:

$$FF_{\text{mean}} = \langle FF \rangle \tag{6}$$

We selected simulated signals from various populations of BNS, NSBH, BBH, and IMBHB systems to check the effectualness of the bank. The details of the simulation sets are summarized in table I. For each signal population, 10^4 simulations were performed.

In Fig. 7, we can see the fitting factors in the M-χ_{eff} plane for BNS aligned-spin TaylorF2 waveform approximants [42] and precessing-spin SpinTaylorT4 waveform approximants [46]. The majority of fitting factors are above 0.97, except along the low-mass edge of the bank at $M = 2.0$ below which no templates are placed. The bank is constructed with aligned-spin TaylorF2 waveforms in this low mass region so fitting factors are expected to be at least as high as the required fitting factor of 0.97 to ensure that no more than $\sim 10\%$ of possible astrophysical signals are lost due to the discrete nature of the bank. We can also see that the majority of fitting factors for precessing-spin SpinTaylorT4 waveform approximants are also above 0.9 although sensitivity falls off rapidly outside $-0.05 < \chi_{\mathrm{eff}} < 0.05$ for systems with NS component mass less than 2 $\mathrm{M}_{\odot}$. There are no templates placed in this region so the fall off in fitting factor is expected. This also demonstrates that a search based on an aligned-spin template bank can recover precessing-spin signals.

In Fig. 8, we can see the fitting factors in the M-χ_{eff} plane and as a function of mass ratio for NSBH aligned-spin SEOBNRv4_ROM waveform approximants [41]. The majority of fitting factors are above 0.97 although fitting factors down to 0.885 are present across this region. Lower fitting factors occur for systems with more extreme mass ratios indicating that the bank is not optimized to recover signals from highly asymmetric systems. A dedicated search in this region may be required to find signals from systems with extreme mass ratios.

In Figures 9 and 10, we can see the fitting factors in M-χ_{eff} plane for BBH and IMBH aligned-spin SEOBNRv4_ROM waveform approximants [41] and as a function of mass ratio for IMBH non-spinning EOBNRv2HM waveform approximants [47]. For the recovery of aligned-spin SEOBNRv4_ROM waveform approximants, the majority of fitting factors are above 0.97. The bank is constructed with SEOBNRv4_ROM waveforms in the high mass region so fitting factors are expected to be at least as high as the required fitting factor of 0.97. We note that fitting factors fall off for high χ_{eff} although coverage in this region is still high. Non-spinning EOBNRv2HM waveform approximants with higher-order modes can also be recovered by the search in the IMBHB region, despite template waveforms not including higher-order mode effects. The fitting factors have a dependency on mass ratios, as higher-order modes become more significant at higher mass ratios. Higher-order modes have higher frequency content and will be within the sensitive frequency band of LIGO and Virgo for IMBH signals. Hence it will become important to include templates containing higher-order modes in their waveforms, in order to increase the sensitivity of the search towards heavier mass systems [48].

IV. CONCLUSION

We have presented the construction and effectualness of the aligned-spin online and offline template banks of gravitational waveforms used by the GstLAL-based inspiral pipeline to analyze data from the second observing run of Advanced LIGO and Virgo. The offline bank expands upon the parameter space covered during the first observing run, including coverage for merging compact binary systems with total mass between $2\,\mathrm{M}_{\odot}$ and $400\,\mathrm{M}_{\odot}$ and mass ratios between 1 and 97.989, thus expanding into the intermediate-mass binary black hole range. The bank requires that templates with component masses less than $2\,\mathrm{M}_{\odot}$ have (anti-)aligned spins between ± 0.05 while component masses greater than $2\,\mathrm{M}_{\odot}$ have allowed (anti-)aligned between ± 0.999. Despite this aligned-spin constraint, we find that the bank can recover some precessing-spin systems. Additionally, higher-order mode effects are not included in the template waveforms but the bank can recover some non-spinning IMBH waveforms with higher-order modes.

We additionally presented a new method that combines a stochastic method with a grid-bank method to better isolate noisy templates at the high mass region of the bank. This allowed for better grouping of templates when performing background estimation.

The online and offline banks played key roles in the to-date discoveries of O2 [3–6] and the offline bank was used in the deep GstLAL reanalysis of O1 and O2 [49]. The experience gained in designing these banks is currently informing the construction of a template bank to be used for the third observing run of Advanced LIGO and Virgo, expected to begin early next year.

V. ACKNOWLEDGEMENTS

Population	Mass($M_\odot$)	Spin	Waveform approximant
BNS	$m_{1,2} \in [1,3]$	$\chi_{1,2} \in [-0.05, 0.05]$, aligned	TaylorF2 [42]
BNS	$m_{1,2} \in [1,3]$	$\chi_{1,2} \in [-0.4, 0.4]$, precessing	SpinTaylorT4 [46]
NSBH	$m_1 \in [1,3]$	$\chi_1 \in [-0.4, 0.4]$, aligned	SEOBNRv4_ROM [41]
	$m_2 \in [3,97]$	$\chi_2 \in [-0.989, 0.989]$, aligned	
BBH	$m_{1,2} \in [2,99]$	$\chi_{1,2} \in [-0.99, 0.99]$ aligned	SEOBNRv4_ROM [41]
IMBHB	$m_{1,2} \in [1,399]$	$\chi_{1,2} \in [-0.998, 0.998]$ aligned	SEOBNRv4_ROM [41]
IMBHB	$m_{1,2} \in [50,350]$	Non-spinning	EOBNRv2HM [47]

TABLE I. Description of different categories of astrophysical populations, from which random mass and spin parameters were drawn and used to generate waveforms to check the effectualness of the template bank. Multiple simulation sets of the same population were used, varying in the type of waveform, mass ranges covered and whether the spin is aligned to the orbital angular momentum.
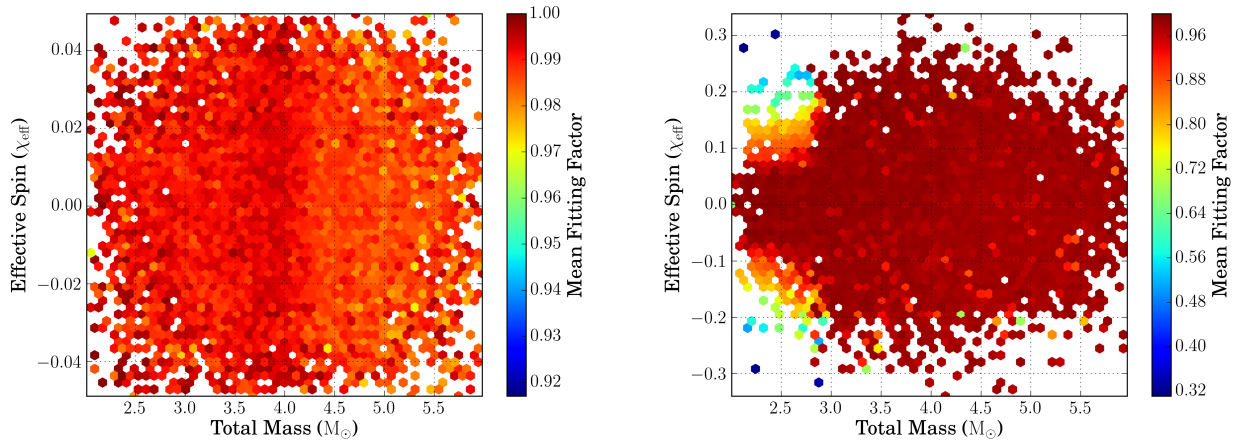

FIG. 7. Fitting factors in M-χ_{eff} plane for BNS aligned-spin TaylorF2 waveform approximants [42] (*left*) and precessing-spin SpinTaylorT4 waveform approximants [46] (*right*). (*Left*) The majority of fitting factors are above 0.97, except along the low-mass edge of the bank at $M = 2.0$ where the fitting factor starts to fall off. The bank is constructed with TaylorF2 waveforms so fitting factors are expected to be at least as high as the required fitting factor of 0.97 to ensure that no more than $\sim 10\%$ of possible astrophysical signals are lost due to the discrete nature of the bank. (*Right*) The majority of fitting factors are above 0.9 although sensitivity falls off rapidly outside $-0.05 < \chi_{\mathrm{eff}} < 0.05$ for systems with NS component mass less than 2 $M_\odot$. There are no templates placed in this region so the fall off in fitting factor is expected. This also demonstrates that a search based on an aligned-spin template bank can recover precessing-spin signals.

[1] B. P. Abbott *et al.* (LIGO Scientific Collaboration and Virgo Collaboration), Phys. Rev. Lett. **116**, 061102 (2016).

[2] A. Albert *et al.* (ANTARES Collaboration and IceCube Collaboration and LIGO Scientific Collaboration, and Virgo Collaboration), Phys. Rev. D **96**, 022005 (2017).

[3] B. P. Abbott *et al.* (LIGO Scientific and Virgo Collaboration), Phys. Rev. Lett. **118**, 221101 (2017).

[4] B. P. Abbott *et al.*, The Astrophysical Journal Letters **851**, L35 (2017).

[5] B. P. Abbott *et al.* (LIGO Scientific Collaboration and Virgo Collaboration), Phys. Rev. Lett. **119**, 141101 (2017).

[6] B. P. Abbott *et al.* (LIGO Scientific Collaboration and Virgo Collaboration), Phys. Rev. Lett. **119**, 161101 (2017).

[7] C. Messick, K. Blackburn, P. Brady, *et al.*, Phys. Rev. D **95**, 042001 (2017).

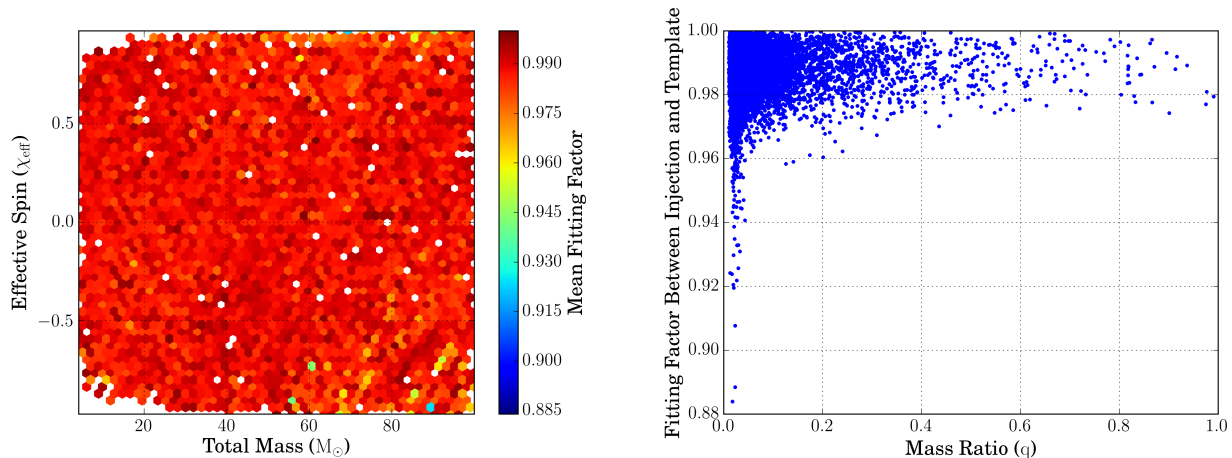[8] K. Cannon, C. Hanna, *et al.*, "Gstlal," `https://www.lsc-group.phys.uwm.edu/daswg/projects/`

FIG. 8. Fitting factors in M-χ_{eff} plane (*left*) and as a function of mass ratio (*right*) for NSBH aligned-spin SEOBNRv4_ROM waveform approximants [41]. (*Left*) The majority of fitting factors are above 0.97 although fitting factors down to 0.885 are present across this region. (*Right*) We can see that the low fitting factors occur for systems with more extreme mass ratios. This indicates that the bank is not optimized to recover signals from highly asymmetric systems.
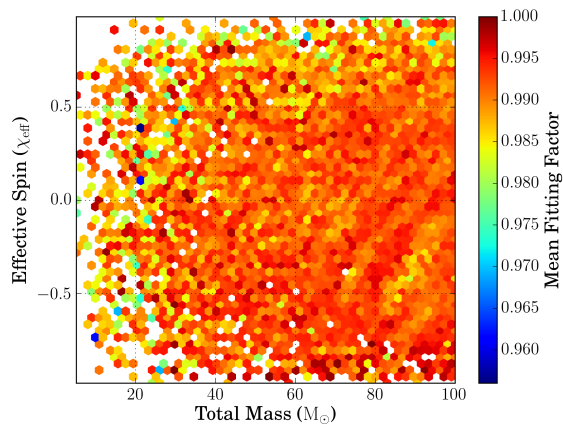

FIG. 9. Fitting factors in M-χ_{eff} plane for BBH aligned-spin SEOBNRv4_ROM waveform approximants [41].

`gstlal.html`, accessed: 2015-07-01.

[9] T. Dal Canton, A. H. Nitz, A. P. Lundgren, *et al.*, Phys. Rev. D **90**, 082004 (2014).

[10] S. Usman, A. H. Nitz, I. W. Harry, *et al.*, Classical and Quantum Gravity **33**, 215004 (2016).

[11] A. H. Nitz *et al.*, "Pycbc software," (2017).

[12] A. H. Nitz, Classical and Quantum Gravity **35**, 035016 (2018).

[13] T. Adams, D. Buskulic, V. Germain, *et al.*, Classical and Quantum Gravity **33**, 175012 (2016).

[14] B. P. Abbott *et al.* (LIGO Scientific Collaboration and Virgo Collaboration), Phys. Rev. D **93**, 122003 (2016).

[15] B. P. Abbott *et al.* (LIGO Scientific Collaboration and Virgo Collaboration), Phys. Rev. X **6**, 041015 (2016).

[16] T. Dal Canton and I. W. Harry, (2017), arXiv:1705.01845 [gr-qc].

[17] B. P. Abbott *et al.* (LIGO Scientific Collaboration and Virgo Collaboration), Phys. Rev. D **96**, 022001 (2017).

[18] C. E. Rhoades and R. Ruffini, Phys. Rev. Lett. **32**, 324 (1974).

[19] V. Kalogera and G. Baym, The Astrophysical Journal Letters **470**, L61 (1996).

[20] F. Özel, D. Psaltis, R. Narayan, and A. S. Villarreal, The Astrophysical Journal **757**, 55 (2012).

[21] J. M. Lattimer, Annual Review of Nuclear and Particle Science **62**, 485 (2012), https://doi.org/10.1146/annurev-nucl-102711-095018.

[22] B. Kiziltan, A. Kottas, M. D. Yoreo, and S. E. Thorsett, The Astrophysical Journal **778**, 66 (2013).

[23] M. Linares, T. Shahbaz, and J. Casares, The Astrophysical Journal **859**, 54 (2018).

[24] F. Özel and P. Freire, Annual Review of Astronomy and Astrophysics **54**, 401 (2016), https://doi.org/10.1146/annurev-astro-081915-023322.

[25] R. O'Shaughnessy, J. Kaplan, V. Kalogera, and K. Belczynski, The Astrophysical Journal **632**, 1035 (2005).

[26] K. Belczynski, A. Buonanno, M. Cantiello, C. L. Fryer, D. E. Holz, I. Mandel, M. C. Miller, and M. Walczak, The Astrophysical Journal **789**, 120 (2014).

[27] S. E. de Mink and K. Belczynski, The Astrophysical Journal **814**, 58 (2015).

[28] M. C. Miller and E. J. M. Colbert, Int. J. Mod. Phys. **D13**, 1 (2004), arXiv:astro-ph/0308402 [astro-ph].

[29] B. P. Abbott *et al.* (Virgo, LIGO Scientific), (2018), arXiv:1808.04771 [astro-ph.CO].

[30] J. W. T. Hessels, S. M. Ransom, I. H. Stairs, P. C. C. Freire, V. M. Kaspi, and F. Camilo, Science **311**, 1901 (2006), astro-ph/0601337.

[31] M. Kramer and N. Wex, Classical and Quantum Gravity **26**, 073001 (2009).

[32] A. C. Fabian, D. R. Wilkins, J. M. Miller, R. C. Reis, C. S. Reynolds, E. M. Cackett, M. A. Nowak, G. G. Pooley, K. Pottschmidt, J. S. Sanders, R. R. Ross, and J. Wilms, Monthly Notices of the Royal Astronomical Society: Letters **424**, 217 (2012), arXiv:1204.5854 [astro-ph.HE].
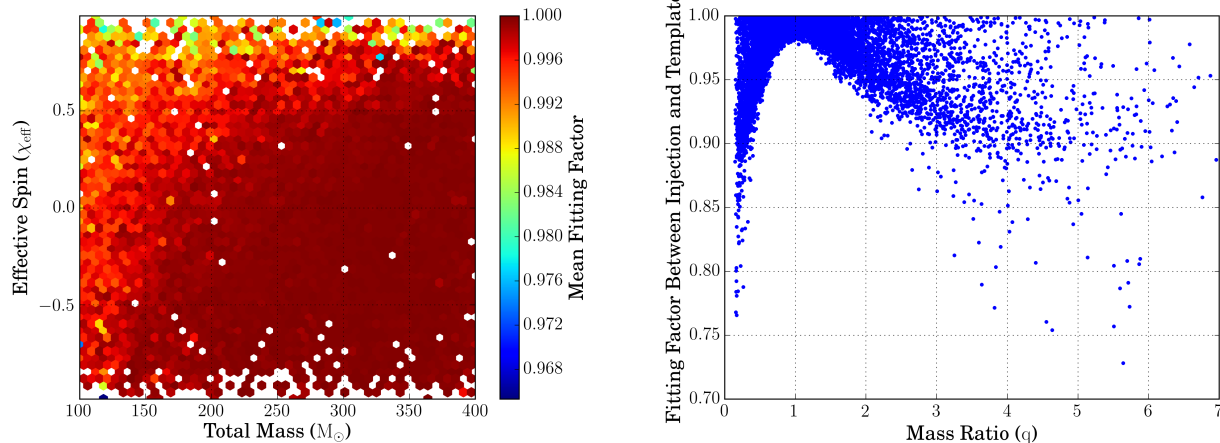
FIG. 10. Fitting factors in M-χ_{eff} plane for IMBH aligned-spin SEOBNRv4_ROM waveform approximants [41] (*left*) and as a function of mass ratio for IMBH non-spinning EOBNRv2HM waveform approximants [47] (*right*). (*Left*) The majority of fitting factors are above 0.97 for the recovery of aligned-spin SEOBNRv4_ROM waveform approximants. The bank is constructed with SEOBNRv4_ROM waveforms in the high mass region so fitting factors are expected to be at least as high as the required fitting factor of 0.97 to ensure that no more than $\sim 10\%$ of possible astrophysical signals are lost due to the discrete nature of the bank. We note that fitting factors fall off for high χ_{eff} although coverage in this region is still high. (*Right*) Non-spinning EOBNRv2HM waveform approximants with higher-order modes can also be recovered by the search in the IMBHB region, despite template waveforms not including higher-order mode effects.

[33] L. Gou, J. E. McClintock, M. J. Reid, J. A. Orosz, J. F. Steiner, R. Narayan, J. Xiang, R. A. Remillard, K. A. Arnaud, and S. W. Davis, Astrophys. J. **742**, 85 (2011), arXiv:1106.3690 [astro-ph.HE].

[34] J. E. McClintock, R. Narayan, S. W. Davis, L. Gou, A. Kulkarni, J. A. Orosz, R. F. Penna, R. A. Remillard, and J. F. Steiner, Classical and Quantum Gravity **28**, 114009 (2011).

[35] C. W. Misner, K. S. Thorne, and J. A. Wheeler, *Gravitation* (W. H. Freeman and Company, 1973).

[36] S. Privitera, S. R. Mohapatra, P. Ajith, K. Cannon, N. Fotopoulos, M. A. Frei, C. Hanna, A. J. Weinstein, and J. T. Whelan, Physical Review D **89**, 024003 (2014).

[37] I. W. Harry, A. H. Nitz, D. A. Brown, A. P. Lundgren, E. Ochsner, and D. Keppel, Phys. Rev. D **89**, 024010 (2014).

[38] T. A. Apostolatos, Phys. Rev. D **52**, 605 (1995).

[39] "aligo sensitivity projections for o2," `https://dcc.ligo.org/LIGO-T1600302` (2017), dcc link.

[40] P. Ajith, N. Fotopoulos, S. Privitera, A. Neunzert, N. Mazumder, and A. Weinstein, Physical Review D **89**, 084041 (2014).

[41] A. Bohé, L. Shao, A. Taracchini, *et al.*, Phys. Rev. D **95**, 044028 (2017).

[42] A. Buonanno, B. R. Iyer, E. Ochsner, Y. Pan, and B. S. Sathyaprakash, Phys. Rev. D **80**, 084043 (2009).

[43] D. A. Brown, I. Harry, A. Lundgren, and A. H. Nitz, Phys. Rev. D **86**, 084017 (2012).

[44] I. W. Harry, B. Allen, and B. S. Sathyaprakash, Phys. Rev. D **80**, 104014 (2009).

[45] "The gstlal search analysis methods for compact binary mergers in advanced ligo's second and advanced virgo's first observing runs," `https://dcc.ligo.org/LIGO-P1700411` (2018), dcc link.

[46] S. Marsat, A. Bohé, L. Blanchet, and A. Buonanno, Classical and Quantum Gravity **31**, 025023 (2014).

[47] Y. Pan, A. Buonanno, M. Boyle, L. T. Buchman, *et al.*, Phys. Rev. D **84**, 124052 (2011).

[48] J. Calderón Bustillo, F. Salemi, T. Dal Canton, and K. P. Jani, Phys. Rev. D **97**, 024016 (2018).

[49] The LIGO Scientific Collaboration and the Virgo Collaboration, arXiv e-prints , arXiv:1811.12907 (2018), arXiv:1811.12907 [astro-ph.HE].